Experimental and DEM study of monotonic and cyclic simple shear testing of an angular sand

Ciantia, Matteo O.; Previtali, Marco; Cakir, Tolga

Published in:
Proceedings of the 20th International Conference on Soil Mechanics and Geotechnical Engineering, Sydney 2021

Publication date:
2022

Document Version
Publisher's PDF, also known as Version of record

Proceedings of the 20th International Conference on Soil Mechanics and Geotechnical Engineering– Rahman and Jaksa (Eds)

Experimental and DEM study of monotonic and cyclic simple shear testing of an angular sand

Étude expérimentale et DEM d'essais de cisaillement monotones et cycliques simples d'un sable angulaire

Matteo O. Ciantia, Marco Previtali & Tolga Cakir
School of Science and Engineering, University of Dundee, United Kingdom, m.o.ciantia@dundee.ac.uk

ABSTRACT: Liquefaction of sandy soils under monotonic and cyclic shear loadings is responsible for numerous devastating failures of earth structures and hence represents a significant hazard. In this paper, cyclic and monotonic loading of an angular sand is replicated in the laboratory using a Cyclic Simple Shear apparatus and numerically using the discrete element method (DEM). For both the experiments and the DEM simulations, undrained conditions were attained by imposing a constant volume approach. A large series of tests, starting from an initial dense state and from two different effective vertical stress conditions, are performed. To obtain a comprehensive Cyclic Stress Ratio (CSR) - number of cycles to liquefaction diagram, from each of these initial states the undrained cyclic tests are conducted using three different shear load magnitudes. The three-dimensional DEM model developed is used to guide the interpretation of the experimental results and to investigate micromechanical processes involved during the cyclic shearing of the angular sand analogue as it approaches liquefaction. To interpret the results using the state parameter (ψ) concept, both drained and undrained monotonic simple shear tests were performed both experimentally and numerically to identify the critical state line.

RÉSUMÉ : *La liquéfaction des sols sableux sous des charges de cisaillement monotones et cycliques est responsable de nombreuses ruptures dévastatrices des structures en terre et représente donc un danger important. Dans cet article, le chargement cyclique et monotone d'un sable angulaire est reproduit en laboratoire en utilisant un appareil de cisaillement simple cyclique dynamique et numériquement en utilisant la méthode des éléments discrets (DEM). Pour les expériences et les simulations DEM, des conditions non drainées ont été atteintes en imposant une approche à volume constant. Une large série d'essais, partant d'un état dense initial et de deux conditions de contraintes verticales effectives différentes, est réalisée. Pour obtenir un diagramme complet du rapport de contrainte cyclique (CSR) - nombre de cycles à liquéfaction, à partir de chacun de ces états initiaux, les essais cycliques non drainés sont effectués en utilisant trois amplitudes de charge de cisaillement différentes. Le modèle DEM tridimensionnel développé est utilisé pour guider l'interprétation des résultats expérimentaux et pour étudier les processus micromécaniques impliqués lors du cisaillement cyclique de l'analogue de sable angulaire à l'approche de la liquéfaction. Pour interpréter les résultats à l'aide du concept de paramètre d'état (ψ), des tests de cisaillement simple monotones drainés et non drainés ont été effectués à la fois expérimentalement et numériquement pour identifier la ligne d'état critique.*

KEYWORDS: Cyclic Simple Shear, Liquefaction, Angular Sands, Particle shape, Discrete Element Method.

1 INTRODUCTION

The Direct Simple Shear (DSS) apparatus is a common laboratory device used to evaluate the element behaviour of soils when subject to simple shear strains (Robinson et al., 2019; Rui et al., 2020). With the aim of recreating a uniform shear strain field for a soil element under in-situ stress states it can probe soil behaviour when principal stress conditions rotate (Wood et al., 1979). Such feature is not possible when using a standard triaxial test device and would require a torsional shear hollow cylinder apparatus (HCA) (Koseki et al., 2005). The advantages of using the HCA are multiple and whilst it is recognised as the most rigorous experimental tool to characterise soils in such conditions, the DSS device is often preferred as sample preparation and testing is simpler and faster. The limitations of this latter are well known and have been matter of several discussions (Airey et al., 1985; Saada et al., 1983). De facto, boundary effects make the element test a boundary value problem and the determination of the stress state within the sample is not a simple task (Wood et al., 1979).

To better understand the stress/strain state within a DSS soil sample, FEM numerical studies providing insight into the mechanism of simple shear were performed several years ago (see e.g. Dounias and Potts, 1993). Thanks to the increase of computational performance, the discrete element method (DEM), which naturally allows granular behaviour to arise through the interaction of rigid particles through simple contact laws, has gained much relevance in geomechanics since originally proposed (Cundall and Strack, 1979). DEM models at the element scale are now widely used as tools of research to investigate and illuminate features of soil mechanics observed in the laboratory (Ciantia et al., 2019). There is also a growing trend to use the DEM to analyse boundary value problems at the element (Boschi et al., 2020), physical modelling (Sharif et al., 2020; Zhang et al., 2021) and field (Boon et al., 2014; Previtali et al., 2021) scale. Bernhardt et al., (2016) showed that DEM simulations can be efficiently and effectively used to study simple shear behaviour of spherical steel spheres. Also Zhang et al., (2019) used DEM simulations to study the bi-directional simple shear response of monodisperse spherical glass beads. Whilst Bernhardt et al., (2016) and Zhang et al., (2019) used spherical particles for their experimental and numerical modelling, Xu et al., (2019) performed a micromechanics investigation of sand gravel mixtures subject to DSS.

In this paper the cyclic simple shear (CSS) response of angular sand is investigated both experimentally, using a variable direction dynamic CSS apparatus, and numerically, by means of DEM modelling. To incorporate particle shape into the DEM model the rolling resistance contact model proposed by Iwashita and Oda, (1998) is employed. Such model introduces a rolling resistance moment, at the contact point proportional to the relative rotation of the contacting particles. Calibration follows the novel approach proposed by Rorato et al., (2021) in which each particle is assigned a sphericity computed through image

analysis. After presenting the image analysis characterization of the sand, drained and undrained simple shear tests/simulations are used to identify the experimental and numerical critical state line (CSL). The CSS experiments and corresponding DEM simulations are then presented. All the simulations presented here were performed using the PFC3D software (Itasca Consulting Group, 2021) .

2 EXPERIMENTAL CHARACTERIZATION

2.1 *Grain size and grain sphericity distributions*

The material employed for the tests is decogravel, an artificial angular dyed silica sand characterized by homogeneous particle size distribution, low sphericity, and a hardness of 7 in the Mohs scale. The particle size distribution (PSD) is determined using both sieving and image analysis, with the former used to validate the latter (Figure 1a). The image analysis uses RGB images, obtained from a standard office scanner. Each RBG image is converted from RGB to HSV (Hue, Saturation and Value), to separate the decogravel grains from the background and binarized through a saturation threshold. Successively, adjacent grains are separated using an inhouse MATLAB coded watershed algorithm (Figure 1b). Following Rorato et al., (2019) the perimeter sphericity of the individual grains (S_P) is calculated as the ratio of the perimeter of a circle of equal area with the particle and the projected perimeter of the particle itself. The true sphericity S is retrieved using the correlation function by Rorato et al., (2019).

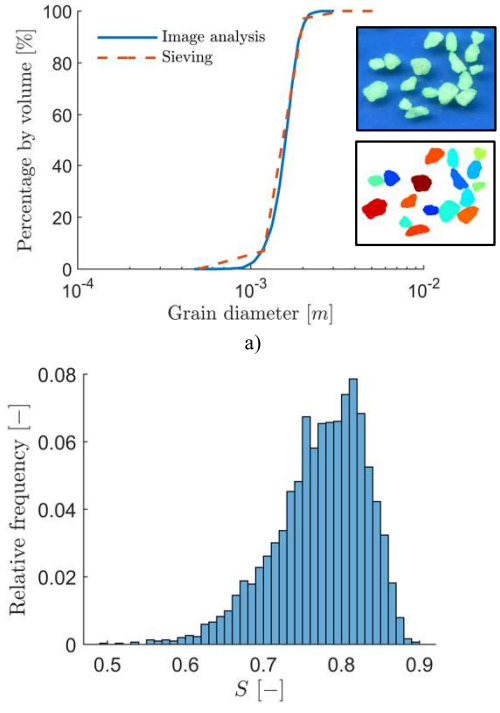

Figure 1 a) PSD of decogravel obtained from sieving and image analysis. (b) Grain sphericity (*S*) distribution from image analysis.

2.2 *Mechanical testing campaign*

The material behaviour is investigated using a Variable Direction Dynamic Cyclic Simple Shear (VDDCSS) apparatus (Figure 2a). The cylindrical sample is characterized by 3 cm height and 7 cm internal diameter and is confined by a series of metallic rings (Figure 2b). The grains are isolated from the rings through an elastic membrane. All decogravel samples, prepared by vibration, are characterized by an initial void ratio of about 0.66. After preparation the samples are placed in the VDDCSS and GDS LVDT local strain transducers are used to measure axial and shear displacements. The samples are consolidated to a vertical stress of 100 or 200 kPa. Drained and undrained (constant volume) displacement controlled shearing tests are performed at these two levels of vertical confining pressure. The undrained CSS tests are carried out in stress control for Cyclic Stress Ratios (CSR) of 0.1, 0.12 and 0.14. Table 1 summarizes the initial conditions of all the tests.

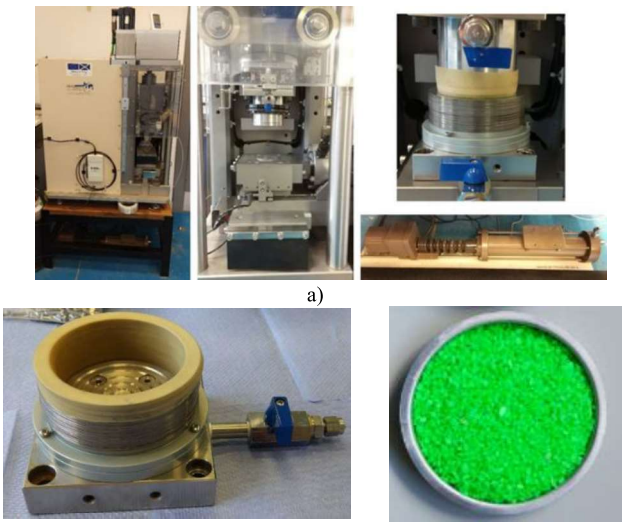

Figure 2 (a) GDS instruments VDDDCS apparatus at the University of Dundee used for the experiments (b) cylindrical sample and picture of ready to test decogravel.

Table 1. Experimental testing details

Test ID	*Loading mode*	e_0	ψ_0	σ_{z0} *[kPa]*	CSR
Exp-SS-D-100	Drained Monotonic	0.65	-0.04	100	-
Exp-SS-D-200	Drained Monotonic	0.63	-0.06	200	-
Exp-SS-U-100	Undrained Monotonic	0.62	-0.07	100	-
Exp-SS-U-200	Undrained Monotonic	0.63	-0.06	200	-
Exp-CSS-U-200-01	Undrained Cyclic	0.64	-0.05	200	0.10
Exp-CSS-U-200-012	Undrained Cyclic	0.64	-0.05	200	0.12
Exp-CSS-U-200-014	Undrained Cyclic	0.64	-0.05	200	0.14

2.2 *Test results*

Figure 3a summarises the all the experimental monotonic shear stress paths in the compression plane ($e - \sigma_z'$) plane while Figure3b reports the same stress paths in the $\tau - \sigma_z'$ plane. These results allowed for an approximate identification of the CSL and the corresponding critical state friction angle. The CSL allowed to estimate the initial state parameter $\psi_0 = e_0 - e_{cs}$ for all the samples. Following Ciantia et al. (2019) the CSL is fitted to the end state points using the following expression

$$e_{cs} = \Gamma + \gamma \left(\frac{\sigma_z'}{100\text{kPa}}\right)^{0.7} \quad (1)$$

giving $\Gamma = 0.69$ and $\gamma = -0.0297$. Figure 4 shows the material response during the undrained CSS tests for the test Exp-CSS-U-200-012. As the number of undrained shear stress cycles increases, the vertical effective stress decreases. When the stress state touches the failure line $\tau = \sigma_z' \tan(\phi)$ the shear strains, which initially remain small and don't show signs of increasing in amplitude, suddenly start to rapidly increase until they diverge and the sample becomes unstable.

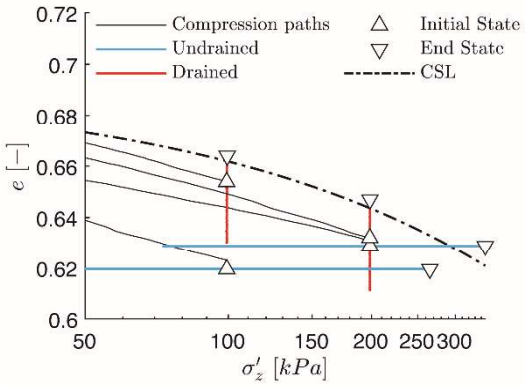

a)

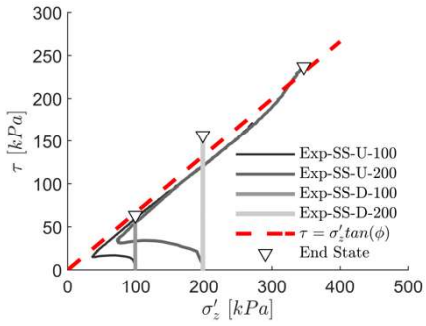

b)

Figure 3 Experimental stress paths in the a) $e - \sigma_z'$ and b) $\tau - \sigma_z'$ planes.

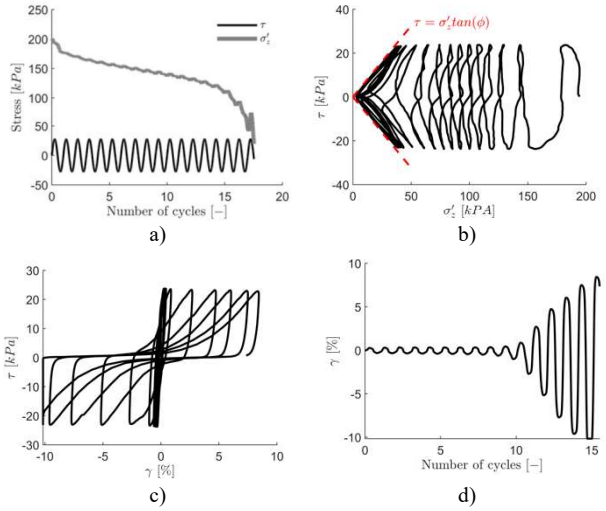

a) b) c) d)

Figure 4 Experimental results of the Exp-CSS-U-200-012 test: a) evolution of τ and σ_z' with number of stress-controlled undrained sharing cycles, b) stress path in the $\tau - \sigma_z'$ plane, c) shear stress-strain response and d) shear strain evolution with number of cycles.

3 MICROMECHANICAL MODELLING

3.1 *DEM contact model for angular sands*

The DEM simulates the behaviour of discrete bodies moving in space following Newton's Laws of Motion, interacting with each other through contact interactions by means of contact models. To account for the low sphericity of the decogravel grains, the rolling resistance contact model (Iwashita and Oda, 1998) is employed. The model, schematically illustrated in Figure 5, includes a conventional linear elastic – frictional contact model for particle relative displacement at the contact plus an additional set of elastic spring no-tensional joint and slider for the rolling motion. Such model introduces a rolling resistance moment, at the contact point proportional to the relative rotation of the contacting particles. This moment can increase up to a maximum limiting value equal to

$$M^* = \mu_r F_n R \tag{2}$$

where μ_r is defined as rolling friction coefficient and F_n is the normal contact force and R is the effective radius ($1/R = 1/R_1 + 1/R_1$ with R_1 and R_2 being the radii of the two particles in contact). Particle stiffness parameters and interparticle contact friction parameters are taken from Rorato et al., (2021) that calibrated a rolling resistance contact model for several silica sands of various shape distributions. Also the rolling friction coefficient was calibrated using the approach proposed by Rorato et al., (2021). Each particle in the model is assigned a sphericity value following the sphericity distribution computed through image analysis (Figure 1). Subsequently, using the mapping function, derived by Rorato et al., (2021)

$$\mu_r = 0.1963(S)^{-8.982} \tag{3}$$

the rolling friction coefficient is then attributed to each particle. The effective rolling friction value of each contact will be the average value of this particle property. The mapping function (eq. 3) was derived by Rorato et al., (2021) by systematically comparing spherical DEM particle rotations with measured grain rotations of a triaxial sand sample.

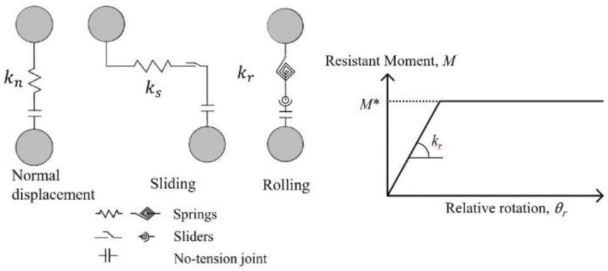

Figure 5 Rolling resistance contact model and elastic-perfectly plastic model accounting for contact rolling resistance (Rorato et al., 2021).

Table 2. DEM model contact parameters

Parameter	*Symbol*	*Value*
Interparticle friction [-]	μ	0.575
Interparticle rolling friction [-]	μ_r	eq. 3
Young Modulus [10^8 Pa]	E_{mod}	4
Normal / shear stiffness ratio [-]	k_{ratio}	2.0
Side walls-particle contact friction [-]	μ_w	0.15
Side walls-particle rolling friction [-]	μ_{rw}	eq. 3*
Horizontal wall-particle friction [-]	μ_w	1.0
Horizontal wall-particle rolling friction [-]	μ_{rw}	eq. 3*

* Same as contacting particle

3.1 *DEM model of CSS*

To model simple shear conditions, instead of replicating the full domain as done by Zhang et al., (2019), periodic boundaries are used in the out-of-plane direction (y axis in Figure 6). In this way a plane strain condition is attained while keeping the total number of particles low for computational efficiency. The model thickness (where the periodic boundaries are used) is taken as 2.5 times the maximum particle diameter, to avoid the limit situation of two particles having multiple contact points through the periodic boundary. The x and z dimensions of the sample are taken as the experiment (7cm and 3cm, respectively). The shearing apparatus is reproduced with two horizontal walls on the upper and lower domain boundaries and two rotating vertical walls on the non-periodic vertical boundaries. The top and the horizontal walls are servo controlled to impose the target stress or strain. Inspired by Han et al., (2018) the sliding (μ) and rolling (μ_r) friction coefficients of the walls are chosen to replicate the laboratory test. In particular a smooth membrane is used in the horizontal walls and a rough-porous steel plate is used for the top wall. Table 2 and Figure 6 summarise and represent the final contact parameters used respectively. The sample, generated using the radii expansion technique (Ciantia et al., 2018) reproduces the PSD shown in Figure 1a. The initial target porosity is higher than the experiential value. Such value was chosen to have a similar ψ_0 before the shearing phase.

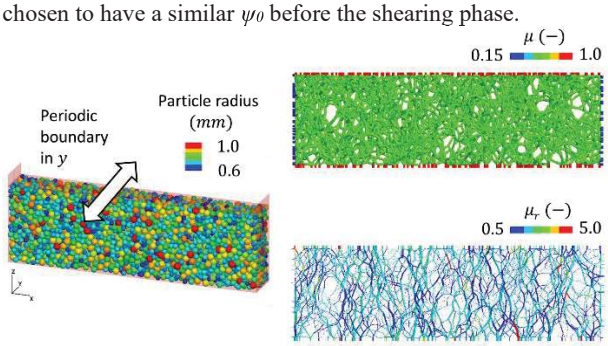

Figure 6 Numerical model for SS plane strain modelling. The contact network shows the contact friction coefficients and the rolling friction used.

Table 3. DEM numerical tests

Test ID	*Loading mode*	e_0	ψ_0	σ_z *[kPa]*	CSR
DEM-SS-D-100	Drained Monotonic	0.75	-0.05	100	-
DEM-SS-D-200	Drained Monotonic	0.74	-0.06	200	-
DEM-SS-U-100	Undrained Monotonic	0.75	-0.05	100	-
DEM-SS-U-200	Undrained Monotonic	0.74	-0.06	200	-
DEM-CSS-U-100-01	Undrained Cyclic	0.75	-0.05	100	0.10
DEM-CSS-U-100-012	Undrained Cyclic	0.75	-0.05	100	0.12
DEM-CSS-U-100-014	Undrained Cyclic	0.75	-0.05	100	0.14
DEM-CSS-U-200-01	Undrained Cyclic	0.74	-0.06	200	0.10
DEM-CSS-U-200-012	Undrained Cyclic	0.74	-0.06	200	0.12
DEM-CSS-U-200-014	Undrained Cyclic	0.74	-0.06	200	0.14

To ensure quasi-static loading conditions (Lopera Perez et al., 2016), the strain rate $\dot{\varepsilon}$ for all DEM tests was such that the number I was always < 10^{-4}. After sample generation and subsequent 1D compression, as for the experiments, drained and undrained (constant volume) displacement-controlled shearing and load-controlled undrained CSS tests were performed. Table 3 summarises the DEM testing campaign. The shear stress is imposed following a sinusoidal curve. The period was selected such that the strain rate was mantling I <10^{-4}.

3.2 *DEM results*

Figure 7a summarises the all the DEM monotonic (drained and undrained) stress paths in the compression plane ($e - \sigma_z'$) plane. The CSL relative to the numerical tests is also represented in the figure. Hereto Eq. (1) is used to fit the data and the two fitting parameters are $\Gamma = 0{,}805$ and $\gamma = -0{,}0108$. The CSL is used to calculate the initial state parameter for the DEM samples (see Table 3). As clearly visible in Figure 3 it was not possible to attain the same initial void ratio e_0 and state parameter contemporaneously. This might be a limitation of using spherical particles and the rolling resistance approach to incorporate particle shape effects. Figure7b shows the numerical stress paths in the $\tau - \sigma_z'$ plane. The experimental Mohr Coulomb failure line is also reported showing a good agreement between the experiments and the DEM.

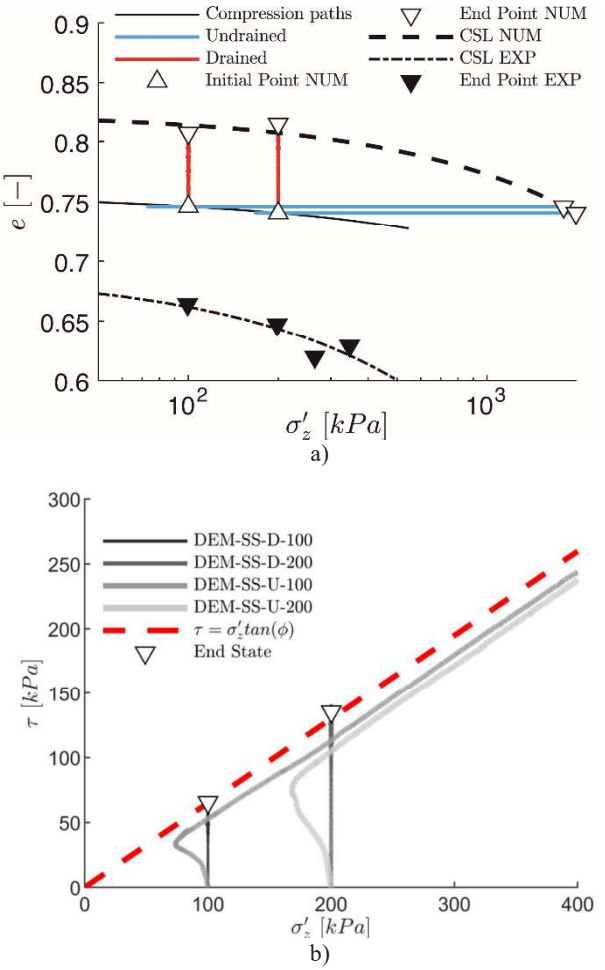

Figure 7 Numerical stress paths in the a) $e - \sigma_z'$ and b) $\tau - \sigma_z'$ planes.

Figure 8a shows the DEM results of the undrained CSS tests for the test DEM-CSS-U-200-012. As the number of undrained shear stress cycles increases, the vertical effective stress decreases. Like for the experiment, when the stress state touches the failure line $\tau = \sigma_z' \tan(\phi)$ the shear strains rapidly increase until liquefaction (Figure 8b).

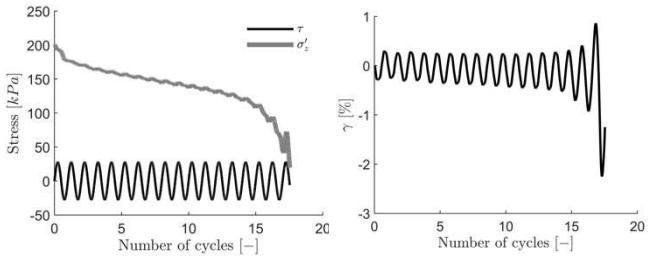

a) b)

Figure 8 Results of the DEM-CSS-U-200-012: a) evolution of τ and σ_z' with number of stress-controlled undrained sharing cycles and b) shear strain evolution with number of cycles.

4 DISCUSSION

Figure 9 compares the experimental and numerical (DEM) number of cycles required to induce liquefaction, with CSR. The results show a relatively good agreement between the two sets of results. The figure also shows how the number of cycles required increases with increasing initial vertical confining stress. It should be noted that, despite the initial void ratio between the experiment and the DEM is different, the initial state parameter ψ_0 is very similar. This might be the reason of the good agreement between the DEM and experiments.

Figure 10 and 11 shows the DEM results of the undrained CSS tests for the test DEM-CSS-U-200-012. As the number of undrained shear stress cycles increases, the vertical effective stress decreases. Like for the experiment, when the stress state touches the failure line $\tau = \sigma_z' \tan(\phi)$ the shear strains rapidly increase until liquefaction (Figure 8b).

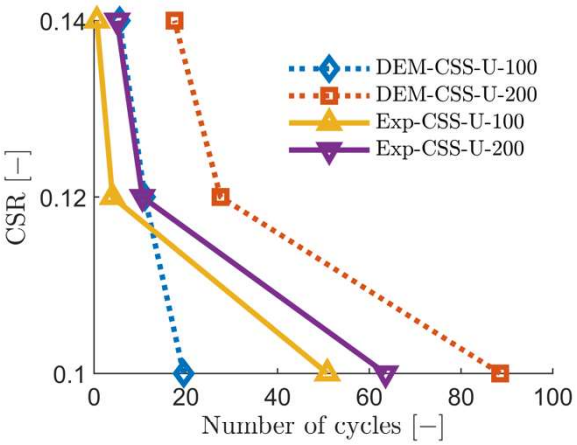

Figure 9 influence of CSR on the number of cycles at liquefaction

Figure 10, 11 and 12 use the data from the DEM-SS-U-200 simulation to highlight how the stress state within the numerical sample rapidly loses homogeneity as shear strains develop. Figure 10 shows how the shear stress measured at the top, at the bottom and within whole sample diverge during the test. Figure 11 compares τ and σ_z' distributions on the top wall as γ increases from 0 (initial state) to 0.1 and 0.2. As shearing progresses it is evident how the stress distribution on the top wall becomes less homogeneous. This is a direct consequence of the force chain distributions that start to cluster into regions of strong (highly loaded) force chains as γ increases (Figure 11). The micromechanical data from the DEM allows to identify that these strong force chains initiate from the bottom left and top right edges (obtuse angles) of the sample to oppose the shear strain. By looking at the particle rotation data, particle rotations are smaller in the highly stressed regions of this strong force chains.

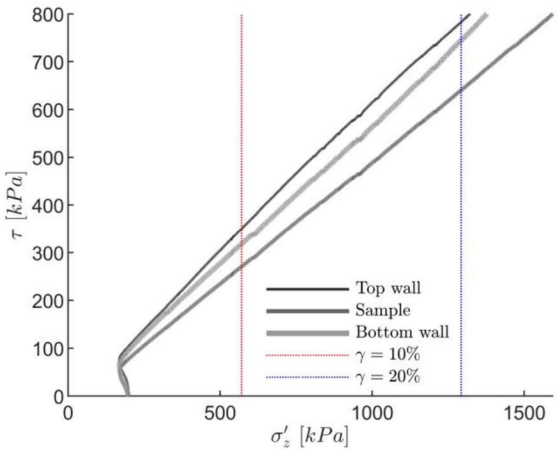

Figure 10 evolution of shear stresses during undrained SS.

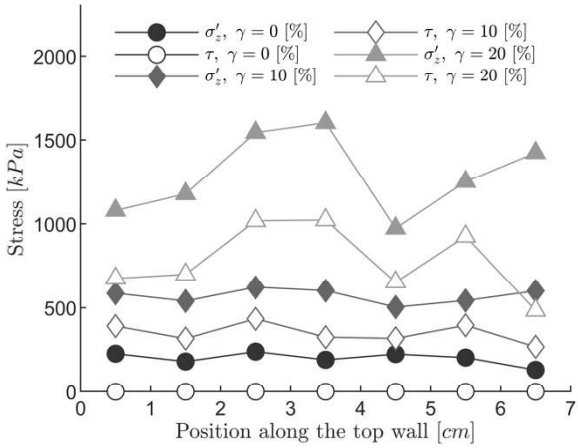

Figure 11 evolution of τ and σ_z' distribution acting on the top wall of the numerical SS apparatus for three levels of deformation

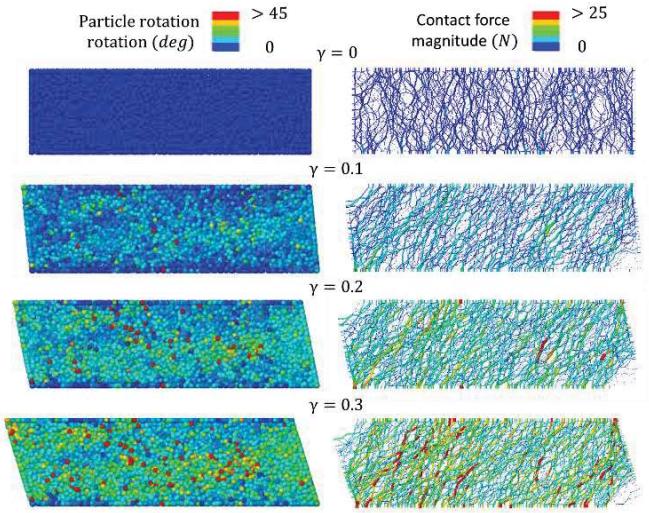

Figure 12 DEM-SS-U-200 particle rotation and contact force chain evolution

5 CONCLUSIONS

This paper presents an experimental and micromechanical numerical analysis of monotonic and cyclic simple shear of an angular sand. To characterise the material experimentally, image analyses are performed to determine grain shape descriptors. The sand is then tested under simple shear conditions by running both drained and undrained monotonic tests. By means of cyclic simple shear tests at three different CSR the number of cycles required to liquefy the sand is determined. The image analysis data is then used to calibrate the rolling friction for the DEM contact model. Plane strain conditions are achieved through periodic boundaries, reducing both the computational burden and the removing the out-of-plane boundary effects caused by the cylindrical rings. The main conclusions form this study are:

i) The angular sands used in this study liquefies when cyclically sheared in undrained (constant volume) conditions. The same sand shows a marked tendency to static liquefaction.
ii) The DEM model can reproduce well the laboratory tests data for all types of loading conditions. Considering that the rolling friction of the DEM contact model is calibrated using 2D grain shape descriptors, this study validates the novel approach proposed by Rorato et al., (2021).
iii) The microscale analysis of the DEM sample during shearing is a very powerful way to improve the current understanding of the widely used DSS apparatus.

6 ACKNOWLEDGEMENTS

The authors would like to thank Dr. Scott Robinson for the fruitful discussions on the VDDCSS apparatus.

7 REFERENCES

Airey, D.W., Budhu, M., Wood, D.M., 1985. Some aspects of the behaviour of soils in simple shear., Developments in soil mechanics and foundation engineering - 2.

Bernhardt, M.L., Biscontin, G., O'Sullivan, C., 2016. Experimental validation study of 3D direct simple shear DEM simulations. *Soils Found*. 56, 336–347.

Boon, C.W., Houlsby, G.T., Utili, S., 2014. New insights into the 1963 Vajont slide using 2D and 3D distinct-element method analyses. *Géotechnique* 64, 800–816.

Boschi, K., di Prisco, C.G., Ciantia, M.O., 2020. Micromechanical investigation of grouting in soils. Int. J. Solids Struct. 187.

Ciantia, M.O., Arroyo, M., O'Sullivan, C., Gens, A., Liu, T., 2019. Grading evolution and critical state in a discrete numerical model of Fontainebleau sand. *Géotechnique* 1–15.

Ciantia, M.O., Boschi, K., Shire, T., Emam, S., 2018. Numerical techniques for fast generation of large discrete-element models. *Proc. Inst. Civ. Eng. - Eng. Comput. Mech*. 171, 147–161.

Cundall, P.A., Strack, O.D.L., 1979. A discrete numerical model for granular assemblies. *Géotechnique* 29, 47–65.

Dounias, G.T., Potts, D.M., 1993. Numerical analysis of drained direct and simple shear tests. *J. Geotech. Eng*. 119, 1870–1891.

Han, F., Ganju, E., Salgado, R., Prezzi, M., 2018. Effects of Interface Roughness, Particle Geometry, and Gradation on the Sand–Steel Interface Friction Angle. *J. Geotech. Geoenvironmental Eng*. 144, 04018096.

Itasca Consulting Group, I., 2021. PFC 6.0.

Iwashita, K., Oda, M., 1998. Rolling Resistance at Contacts in Simulation of Shear Band Development by DEM. *J. Eng. Mech.*

Koseki, J., Yoshida, T., Sato, T., 2005. Liquefaction properties of Toyoura sand in cyclic tortional shear tests under low confining stress. *Soils Found*. 45, 103–113.

Lopera Perez, J.C., Kwok, C.Y., O'Sullivan, C., Huang, X., Hanley, K.J., 2016. Assessing the quasi-static conditions for shearing in granular media within the critical state soil mechanics framework. *Soils Found*. 56, 152–159.

Previtali, M., Ciantia, M. O., Spadea, S., Castellanza, R. and Crosta, G. B. (2021) Multiscale modelling of dynamic impact on highly deformable compound rockfall fence nets, *Proc. Inst. Civ. Eng. - Geotechnical Engineering*. AoP

Robinson, S., Brennan, A., Knappett, J., Wang, K., Bengough, G., 2019. Cyclic simple shear testing for assessing liquefaction mitigation by fibre reinforcement. In: Silvestri, F., Moraci, N. (Eds.), Earthquake Geotechnical Engineering for Protection and Development of Environment and Constructions, Proceedings in Earth and Geosciences. CRC Press, pp. 4728–4735.

Rorato, R., Arroyo, M., Andò, E., Gens, A., 2019. Sphericity measures of sand grains. *Eng. Geol.* 254, 43–53.

Rorato, R., Arroyo, M., Gens, A., Andò, E., Viggiani, G., 2021. Image-based calibration of rolling resistance in discrete element models of sand. *Comput. Geotech.* 131, 103929.

Rui, S., Guo, Z., Si, T., Li, Y., 2020. Effect of particle shape on the liquefaction resistance of calcareous sands. *Soil Dyn. Earthq. Eng.* 137, 106302.

Saada, A.S., Fries, G., Ker, C.C., 1983. Evaluation of laboratory testing techniques in soil mechanics. *Soils Found.* 23, 98–112.

Sharif, Y.U., Brown, M., Ciantia, M.O., Cerfontaine, B., Davidson, C., Knappett, J., Meijer, G.J., Ball, J.D., 2020. Using DEM to create a CPT based method to estimate the installation requirements of rotary installed piles in sand. *Can. Geotech. J.* cgj-2020-0017.

Wood, D.M., Drescher, A., Badhu, M., 1979. On the determination of stress state in the simple shear apparatus. *Geotech. Test. J.* 2, 211–222.

Xu, D.S., Tang, J.Y., Zou, Y., Rui, R., Liu, H.B., 2019. Macro and micro investigation of gravel content on simple shear behavior of sand-gravel mixture. *Constr. Build. Mater.* 221, 730–744.

Zhang, M., Yang, Y., Zhang, H., Yu, H.-S., 2019. DEM and experimental study of bi-directional simple shear. *Granul. Matter* 21, 24.

Zhang, N., Arroyo, M., Ciantia, M.O., Gens, A., 2021. Energy balance analyses during Standard Penetration Tests in a virtual calibration chamber. *Comput. Geotech.* 133, 104040.